Solar Phys (2012) 281:779–792
DOI 10.1007/s11207-012-0096-4

Coronal Mass Ejections and the Index of Effective Solar Multipole

V.N. Obridko · E.V. Ivanov · A. Özgüç · A. Kilcik · V.B. Yurchyshyn

Received: 17 February 2012 / Accepted: 30 July 2012 / Published online: 21 August 2012

Abstract The paper considers the relationship between the cyclic variations in the velocity of coronal mass ejections (CME) and the large-scale magnetic field structure (LSMF) in cycles 21 – 23. To characterize a typical size of the LSMF structure, we have used the index of the effective solar multipole (ESMI). The cyclic behavior of the CME occurrence rate and velocity proved to be similar to that of ESMI. The hysteresis observed in variations of the CME maximum velocity is interpreted as a manifestation of different contributions from the two field structures (local and global magnetic fields) in different phases of the 11-year activity cycle. It is suggested that cyclic variations in the maximum velocity of coronal mass ejections are due to different conditions for the formation of the complexes of active regions connected by coronal arch systems, which are the main source of high-velocity CMEs.

1. Introduction

The cyclic variation of solar activity is usually characterized by specific indices associated with local magnetic fields. The primary index that allowed the phenomenon of solar activity to be discovered was the Wolf sunspot number. Other widely used indices are the sunspot area, the numbers of flares and radio bursts, the characteristics of active regions, faculae, and flocculi, as well as the integrated flux in radio, X-rays, and UV. All indices and their various combinations are determined by local magnetic fields. At the same time, there is an obvious deficit of indices to characterize cyclic variations of the structure and energetics of global magnetic fields. In some studies (*e.g.*, see Makarov and Sivaraman 1989a, 1989b; Hoeksema

V.N. Obridko (✉) · E.V. Ivanov
Pushkov Institute of the Terrestrial Magnetism, Ionosphere and Radiowave Propagation RAS (IZMIRAN), 142190 Troitsk, Russian Federation
e-mail: obridko@izmiran.ru

A. Özgüç
Kandilli Observatory and Earthquake Research Institute, Bogazici University, 34684 Istanbul, Turkey

A. Kilcik · V.B. Yurchyshyn
Big Bear Solar Observatory, Big Bear City, CA 92314, USA

and Scherrer, 1986) the cyclic variations of global and background fields have been investigated (Obridko and Shelting, 1992). By 'local fields' we shall, henceforth, mean the fields with characteristic spatial scale comparable with the size of a developed active region, and by 'global fields' the fields with characteristic spatial scale comparable to the solar radius. In this paper, we briefly touch upon the intermediate-scale fields called 'background fields', and we will not mention at all the fields of smaller scale than local fields.

Many authors (Bumba 1976, 1986; Bumba and Gesztelyi, 1988; Ivanov 1986, 1994, 1995; Kuklin, 1971; Kuklin and Obridko, 1989; Obridko, 1984) have shown in their work that:

i) There are two systems of magnetic fields existing in the Sun that differ in their evolution, rotation, and energy characteristics (see Bumba, 1986; Ivanov 1986, 1994). There is a lot of evidence that these systems are associated with global and local fields whose interplay determines the main variety of solar active phenomena.
ii) The long-term characteristics of solar activity are determined by global fields, both directly and through their effect on local fields (active longitudes, complexes of activity, impulses of activity, *etc.*). Of course, there is also a reverse effect of local fields on the global ones.
iii) It is the structure of global fields that determines the energetics and occurrence rate of many geomagnetic and interplanetary events.

What then are the indicators of the global field structure? First of all, these are coronal holes. These structures are determined by the entire pattern of large-scale magnetic field distribution on the Sun which manifests itself in the corona and in the interplanetary space, and they are closely associated with high-velocity streams and the IMF (interplanetary magnetic field) sector structure (Obridko and Shelting, 1987, 2011; Shelting and Obridko, 1988; Obridko *et al.*, 2009). Other features indicative of the global magnetic field structure are the complexes of several active regions connected by coronal arches. Since, as shown earlier (Bumba and Obridko, 1969; Ivanov, 2007), major sunspots and active regions are concentrated at the cell boundaries of the large-scale solar magnetic field, the size of such complexes is closely related to the size of the corresponding elements (cells) of the latter. To characterize these structural elements, Ivanov, Obridko, and Shelting (1997) introduced the index of effective solar multipole (ESMI).

2. Energy Indices of the Global Magnetic Field

A quantitative index that can be introduced for global fields is the energy index. For analyzing cyclic variations of the global solar magnetic field, it is convenient to introduce magnetic indices which are quantities defined by the global distribution.

Let $i(B_r)$ denote the square of the radial component of the magnetic field averaged over the solar surface:

$$i(B_r)|_R = \left\langle B_r^2 \right\rangle, \tag{1}$$

where R is the radius of the sphere over which the averaging is performed. In order to calculate $i(B_r)$, one should know the magnetic field B_r. We have used magnetic field data obtained at the Wilcox Solar Observatory, Stanford, with a 3 arcmin resolution. Their representation in the form of Legendre polynomials has been used

$$B_r = \sum_{lm} P_l^m(\cos\theta)(g_{lm}\cos m\phi + h_{lm}\sin m\phi) \times \left\{(l+1)\left[\frac{R_\odot}{R}\right]^{l+2} + l\left[\frac{R}{R_S}\right]^{l-1}\zeta^{l+2}\right\} \quad (2)$$

where l and m are the indices of spherical harmonics, $\zeta = R_\odot/R_S$ and $R_\odot$ is the radius of the Sun, $R_S = 2.5\ R_\odot$ is the radius of the source surface, P_{nm} is the Legendre polynomial; g_{lm} and h_{lm} are calculated based on the Stanford data (http://wso.stanford.edu/). We are using synoptic charts of the line-of-sight component of the magnetic field available at the above-mentioned site. Each synoptic chart contains 2160 points. From the general solution, we obtain a theoretical expression for the line-of-sight component with unknown coefficients g_{lm} and h_{lm}. Setting the theoretical expression equal to that obtained from observations, we find the coefficients g_{lm} and h_{lm}. Here, the values of g_{lm} and h_{lm} can be found either proceeding from the orthogonal property of the Legendre polynomials, or directly by the least square method. Both methods give similar results. Then, knowing the coefficients g_{lm} and h_{lm}, we can calculate the magnetic field.

For the surface of the photosphere ($R = R_\odot$) and the source surface ($R = R_S$) we have, respectively,

$$B_r|_{R_\odot} = \sum_{lm} P_l^m(\cos\theta)(g_{lm}\cos m\phi + h_{lm}\sin m\phi)\left(l+1+l\zeta^{2l+1}\right), \quad (3)$$

$$B_r|_{R_s} = \sum_{lm} P_l^m(\cos\theta)(g_{lm}\cos m\phi + h_{lm}\sin m\phi)(2l+1)\zeta^{l+2}. \quad (4)$$

If we apply the averaging procedure (Equation (1)) to Equations (3) and (4) we obtain the following expressions for the indices $i(B_r)|_{R_\odot}$ and $i(B_r)|_{R_s}$ (Obridko and Ermakov, 1989):

$$i(B_r)|_{R_\odot} = \sum_{lm} \frac{(l+1+l\zeta^{2l+1})^2}{2l+1}(g_{lm}^2 + h_{lm}^2), \quad (5)$$

$$i(B_r)|_{R_s} = \sum_{lm} (2l+1)\zeta^{2l+4}(g_{lm}^2 + h_{lm}^2). \quad (6)$$

We have proposed an index of the effective solar multipole (ESMI; Ivanov, Obridko, and Shelting 1997, 1998; Ivanov *et al.*, 1999):

$$\mathrm{ESMI} = -0.5\log(I_s/I_\odot)/\log(2.5), \quad (7)$$

where I_s and $I_\odot$ are the values of $i(B_r)$ at the source surface ($r = 2.5R_\odot$) and on the photosphere ($r = R_\odot$), respectively.

The variation of ESMI shows that the contribution from different components of the global magnetic field (*i.e.* systems of giant and supergiant granules) to the integrated magnetic flux changes during a solar cycle. In fact, when passing from the photosphere to the source surface, the magnetic flux changes in accordance with the formula $B_s = B_\odot r^{-\mathrm{ESMI}}$, where ESMI = 3 for a dipole source (global field), ESMI = 4 for a quadrupole source (intermediate scale field), and ESMI > 4 for a higher-order multipole source (local fields). When the field under consideration is produced by several sources combined with different weight, ESMI can assume values from three to four (in the case of combined dipole and quadrupole sources) or higher (in the case of a higher-order multipole field). Therefore, we may also call EMSI the multipole index hereafter.

The calculation procedure was described, in particular, in Obridko and Ermakov (1989) and in Obridko and Kuikin (1993). The advantage of this index is that it can be related to various magnetic systems in the Sun.

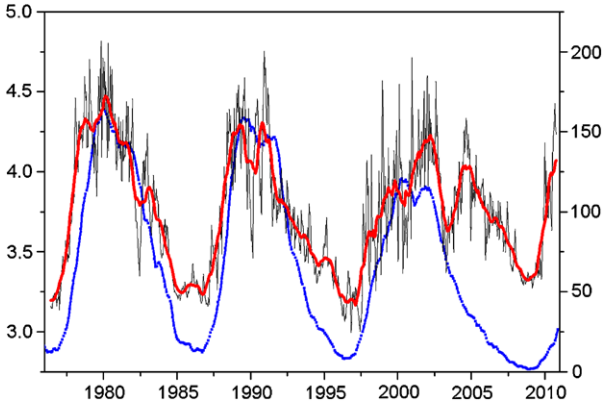

Figure 1 The multipole index ESMI (black and red) and the monthly sunspot number SSN smoothed over 13 months (blue). Each black data point corresponds to a Carrington rotation, while the red curve is smoothed over 13 rotations.

In Figure 1, the multipole (EMSI) index is compared with the smoothed sunspot number (SSN). The black curve shows the values of ESMI for each Carrington rotation, the red curve illustrates the ESMI values smoothed over 13 rotations, and the blue curve corresponds to the monthly mean SSN values smoothed over 13 months. As seen from Figure 1, the multipole index becomes significant in the rising phase and remains so during the whole maximum phase. Then its value decreases and becomes equal to ≈ 3 at the minimum of the cycle.

Three particularities should be emphasized:

i) The secondary maximum is much more pronounced in ESMI than in SSN. This may imply that the contribution from the medium-scale fields to the secondary maximum is more significant.
ii) In the declining phase, the variation of the multipole index (ESMI) may differ significantly from that of SSN. In particular, in the anomalous cycle 23, the decrease in ESMI down to the dipole value in 2003 was reversed by a new considerable increase, which was, obviously, due to an increase in the magnetic-field multipole component (and a corresponding decrease in the characteristic size of elements of the large-scale solar magnetic field (LSMF)). This caused a drastic increase in the number of equatorial coronal holes (Tokumaru *et al.*, 2009) and in the number of relatively large complexes of activity that consist of a few active regions responsible for intensive high-speed CMEs.
iii) The variation of the ESMI index shows that the maximum values of ESMI were decreasing continuously (and the size of the LSMF cells was increasing correspondingly) at the cycle maxima during the past three activity cycles.

The ESMI index we have introduced earlier allows us to describe the cycle variation in terms of the contributions from fields of different scales. The varying contributions from different field scales play a crucial part in describing the solar periodicity. We have established that the main phenomena of solar activity, such as active regions, sunspot groups, and flares, show a tendency to concentrate at the boundaries of LSMF structural elements. This trend manifests itself in the occurrence of the so-called active longitudes (Bumba and Obridko, 1969; Ivanov, 2007). The concentration along the active longitudes and IMF sector boundaries increases with the intensity (importance) of the active events and is most clearly pronounced in the case of major events (*e.g.*, X-ray and proton flares). On the other hand, numerous minor sunspots do not display any concentration at the active longitudes (Ivanov, 2007).

Kilcik *et al.* (2011b) analyzed the cyclic variation of sunspot numbers and their total areas for the past four solar cycles (cycles 20 – 23) separately for minor sunspots (Zurich

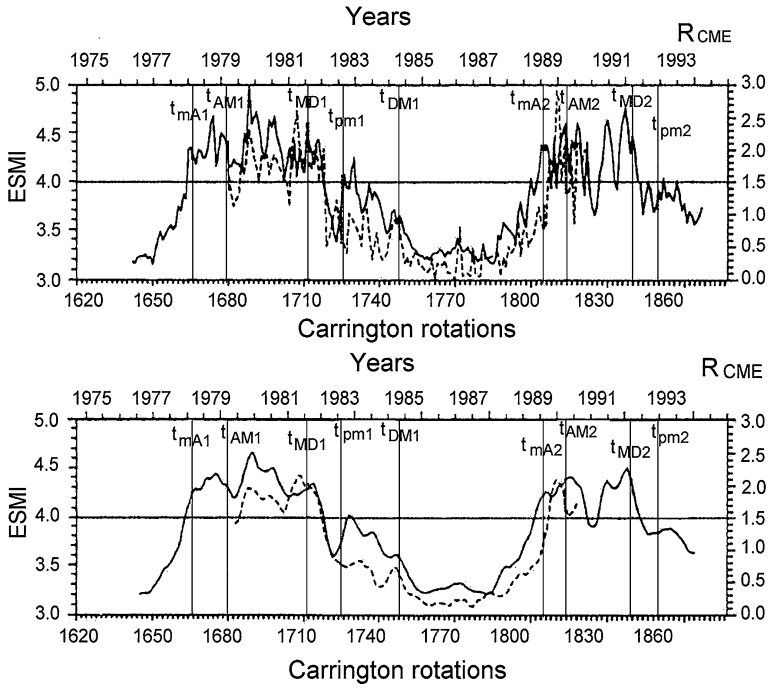

Figure 2 The upper panel shows daily mean CME occurrence rates for 1979 – 1989 averaged over a Carrington rotation (solid line) (Ivanov, Obridko, and Shelting, 1997) and variation of ESMI (dotted line) for cycles 21 and 22. The lower panel is the same after smoothing over six rotations. Various times (t_{mA} and others) are defined in the text.

classes A, B, C, H, and J) and for major complex sunspot groups (classes D, E, F, and G). The cyclic curves for both groups of sunspots proved to differ noticeably. Moreover, the curves for the 10.7-cm radio flux, facular areas, and CME maximum velocities were shown to agree with the curves for most complex sunspot groups much better than with those for minor sunspots.

3. The Multipole Index and Cyclic Variation of CME Number

Now, let us turn to a direct comparison of cyclic variations of the CME occurrence rate and the multipole index characterizing the relative contribution from the fields of different scales.

Figure 2 represents the daily mean CME rates averaged over a Carrington rotation for the period of 1979 – 1989 and ESMI variation for the same period. The figure also shows the solar cycle reference points: the beginning and end of the epoch of minimum (t_{DM} and t_{mA}) and the beginning and end of the epoch of maximum (t_{AM} and t_{MD}). These reference points were introduced by Vitinsky, Kuklin, and Obridko (1986). Later, Danilchev, Morozova, and Obridko (1986) introduced an additional reference point – pre-minimum (t_{pm}).

The curves on Figure 2 display a good agreement. The correlation coefficient is 0.83 and increases up to 0.94 after smoothing over six rotations. This suggests a close relationship between the structural variations of large-scale solar magnetic fields (ESMI variations) and the CME occurrence rate.

These variations are, apparently, associated with the character of changes in the global magnetic systems. The energy of each system increases or decreases during a cycle, and the energy distribution between the systems changes with the phase of the cycle. With activation of the systems of local and medium-scale fields, the CME occurrence rate increases abruptly. Conversely, a decrease in ESMI to the values smaller than four, which indicates a decrease in energy and relative contribution from the multipole component to the solar magnetic flux, results in a similar decrease in the CME occurrence rate.

4. The Multipole Index and Cyclic Variation of CME Speed in Cycle 23

Studies of the relationship between different coronal activity indices during the solar cycle may provide evidence about the storage of energy in the corona. Donnelly (1992) has shown that some of these activity indicators such as 10.7 cm solar radio flux, Ca II K index, and Lα irradiance at 1216 Å follow different paths for the ascending and descending phases of the solar cycle, displaying a 'hysteresis'-like phenomena. In some cases, these observed hysteresis patterns start to repeat over more than one solar cycle, giving evidence that this is a normal feature of solar activity. This was interpreted in terms of active regions evolving from the photosphere upward.

Özgüç and Ataç (2002) extended this analysis to include the variation of the Hα flare index (FI), as well as some other solar activity indices (sunspot number (SSN), total sunspot area (SSA), solar radio flux at 10.7 cm (F10.7), flare index (FI), coronal index (CI), total solar irradiance (TSI), and mean magnetic field) over three solar cycles (20, 21, and 22). They found that the hysteresis effects are irregular over the three solar cycles.

Kilcik *et al.* (2011a) introduced a new index called Maximum Coronal Mass Ejection Speed Index (MCMESI) and they found that this new indicator better reflects geomagnetic activity than other solar activity indicators such as SSN, SSA, FI, *etc*.

Figure 3a represents the cyclic variation of our ESMI (multipole) index in cycle 23 (thick black curve). Also plotted are the maximum speed $V_{\max}$ (red) and the mean speed V (blue) of CMEs. Hereinafter, the values of V, $V_{\max}$, and n (CME occurrence rate) are calculated for all CME events entered in the LASCO list (http://cdaw.gsfc.nasa.gov/CME_list). All values of n, $V_{\max}$, and V were calculated at a step equal to half a Carrington rotation (≈ 13.5 days) and then smoothed over a year. Given that CMEs are randomly distributed in direction from the Earth's perspective, any projection effects would average out. Therefore, the projection effects were not taken into account. Though the $V_{\max}$ curve was calculated for the CME maximum velocities over a period of ≈ 13.5 days (1/2 Carrington rotation), it agrees fairly well with the curve obtained by Özgüç, Kilcik, and Rozelot (2012) for daily data.

Figure 3b illustrates the cross-correlation between ESMI and $V_{\max}$ (solid line) and between ESMI and V (dashed line). The abscissa shows the shift of the cross-correlation function in the units equal to half a Carrington rotation (one year comprises approximately 27 such units). Owing to their multiplicity, the low-speed CMEs make the basic contribution to the mean CME velocity V. As seen from these figures, the variations of the large-scale magnetic field structure (ESMI) and CME maximum velocity ($V_{\max}$) are closely related and occur virtually without any time delay, while the variations of the mean CME velocity (V) precede those of ESMI by about 2 years.

Figure 4a represents cyclic variations of the ESMI (multipole) index in a solid line and the CME occurrence rate (*i.e.*, the number of CME events observed during an interval of ≈ 13.5 days, which corresponds to half a Carrington rotation) in a dashed line. In Figure 4b, we show the cross-correlation between ESMI and the CME occurrence rate over the activity

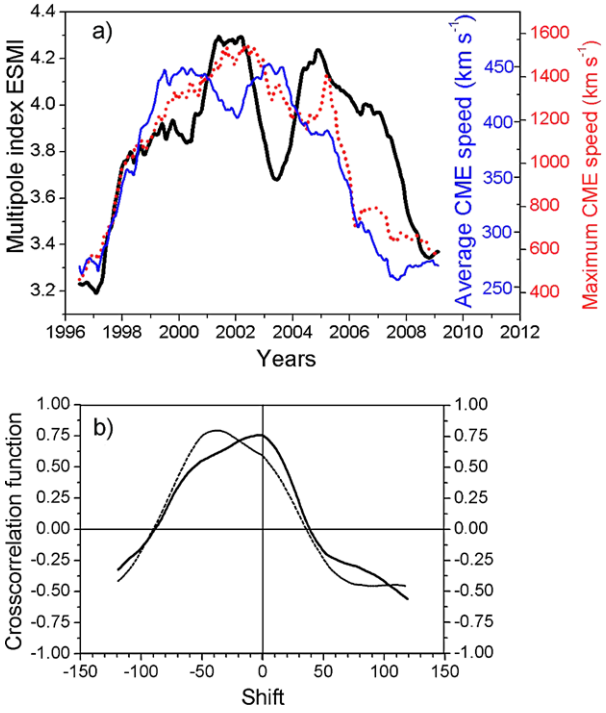

Figure 3 (a) Cyclic variations of the ESMI (multipole) index (black) and the maximum (V_{max}, red) and mean (V, blue) CME velocities in cycle 23. (b) Cross-correlation between ESMI and V_{max} (solid) and between ESMI and V (dashed) in cycle 23.

cycle 23. Again, one can see a clearly pronounced relationship between the large-scale field structure and CME occurrence rate with a shift of about 0.6 year.

As seen from Figure 3, the maximum ESMI values correspond to the largest values of the CME maximum velocity. One scenario to explain this correlation is that the decrease in the field elements (increase in ESMI) favors the appearance of a relatively large unipolar region, clustering of large sunspot groups (active regions) at its boundaries, and formation of a single complex of several active regions joined by coronal arch systems. When this complex exists for a long time, the effect of an active longitude occurs. In this case, a CME accompanied by the ejection of an arch system will result in the appearance of a dimming on the place of the latter with a size determined by the size of the previously existing arch system. When the size of the field elements increases in the declining phase of the cycle (*i.e.*, when ESMI decreases), the formation of a large active complex becomes less likely. The number of active regions involved in the formation of a complex and, hence, the energy of the latter decrease. As a result, the maximum velocity of CME decreases correspondingly. At the end of the declining phase (2007 – 2009), when the characteristic size of the LSMF elements increased significantly, the formation of complexes of several AR and the occurrence of intensive, high-speed CMEs became impossible. At this time, the occurrence of weak, low-speed CMEs in relatively small sources (sunspots and eruptive filaments) increased. This concept is supported by various authors (Zhang *et al.*, 2007; Chertok and Grechnev, 2005; Chertok, Belov, and Grechnev, 2011; Grechnev *et al.*, 2005; Reinard and Biesecker, 2009). For example, Zhang *et al.* (2007) studied four major high-speed halo CMEs (14 July 2000, 28 October 2003, 7 November 2004, and 15 January 2005) and revealed that more than ten different magnetic arch systems joining several active regions were involved in CME production. Although the dimming events are often present behind CMEs even when the magnetic configuration is relatively simple, there is evidence that they are, in many cases,

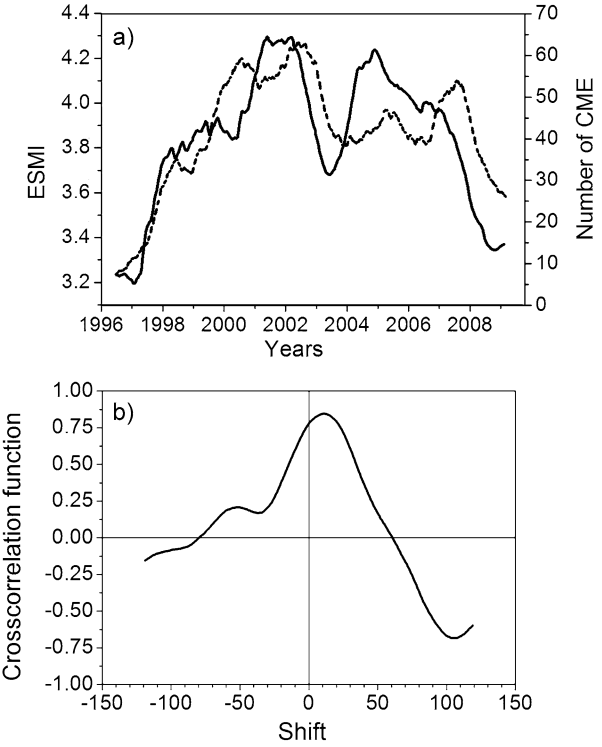

Figure 4 (a) Cyclic variations of the ESMI (multipole) index (solid) and the CME occurrence rate (dashed) in cycle 23. (b) Cross-correlation between ESMI and CME occurrence rate in cycle 23.

associated with arch systems. Chertok and Grechnev (2005) and Grechnev *et al.* (2005) showed that the dimming events arising at the place of powerful CMEs were preceded by arch systems that had joined several active regions. The same authors (Chertok, Belov, and Grechnev, 2011) found that the CME velocity increased with the increase of the magnetic flux in the dimming (determined to a large extent by the area of the latter). Reinard and Biesecker (2009) established also that the CME events accompanied by dimming had higher velocities than the CMEs without dimming.

5. The Multipole Index and Cyclic Variation of CME Speed in Cycles 21 – 22

Figure 5 illustrates a) the cyclic variation of ESMI (black) and the maximum (V_{max}) and mean (V) CME velocities (red and blue, respectively) for the declining phase of cycle 21 (1979 – 1984) and the rising phase of cycle 22 (1984 – 1989) and b) the CME occurrence rate (n, magenta) compared to ESMI (black) for the same time interval. The same as in Figures 3 and 4, all values of ESMI, V_{max}, V, and n were calculated at a step equal to half a Carrington rotation ($\approx$ 13.5 days) and were then smoothed over a year. The data for 1979 – 1984 were obtained from the *Solwind* satellite (http://lasco-www.nrl.navy.mil/solwind_transient.list) (Howard *et al.*, 1991) and the data for 1984 – 1989 from the *Solar Maximum Mission* (SMM; Burkepile and St. Cyr, 1993). Since the coronagraphs installed on board the *Solwind* and SMM spacecraft were less sensitive than the SOHO coronagraph (LASCO), they recorded much fewer weak (low-speed) CME events than LASCO did (compare the n curves in Figures 4a and 5). As a result, the contribution from intensive events to the CME mean velocity

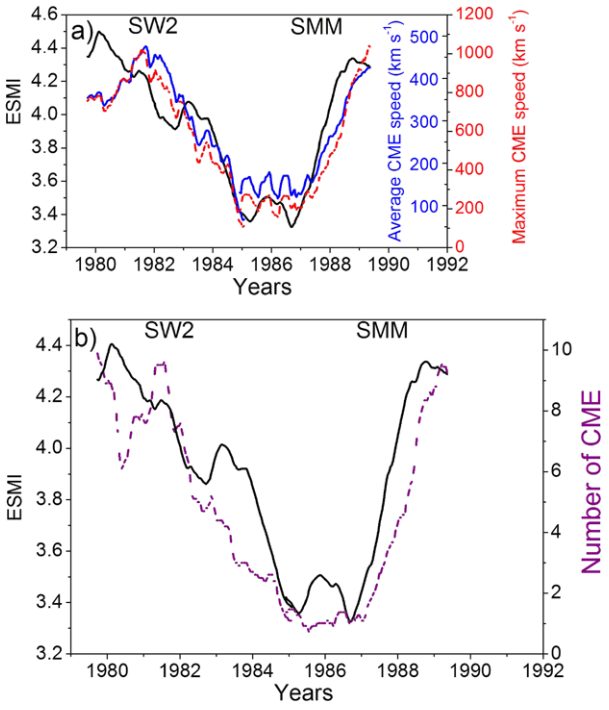

Figure 5 (a) Cyclic variations of the ESMI (multipole) index (black) and the maximum (V_{max}, red) and mean (V, blue) CME velocities for the declining phase of cycle 21 (1979 – 1984) and the rising phase of cycle 22 (1984 – 1989). (b) The CME occurrence rate (n, magenta) compared to ESMI (black) for the same time interval.

was predominant in the *Solwind* and SMM data. Therefore, unlike the period of 1996 – 2009, the cyclic curves for the CME maximum and mean velocities for the period of 1979 – 1989 correlate fairly well without a time shift. Otherwise, such as in Figures 3 and 4, the largest values of the CME maximum velocity correspond to the largest values of ESMI and n.

Since the data for the declining phase of cycle 21 and the rising phase of cycle 22 were obtained from different space missions, a quantitative comparison between the CME maximum velocity and ESMI was performed separately. The comparison revealed an unexpected result. On the ascending branch of cycle 22, all curves display a high correlation with a coefficient of 0.98 – 0.99 and a small time shift from 3 months to half a year. The precise delay time is difficult to estimate, because the cross-correlation functions have flat peaks, and the correlation coefficient changes insignificantly with the change of the shift. The situation is quite different on the descending branch of cycle 21.

Figure 6a shows V_{max} as a function of ESMI for the ascending branch of cycle 22. The points follow at intervals equal to half a Carrington rotation ($\approx$ 13.63 days). The velocity data are shifted back in time by 14 half-rotations. The linear correlation coefficient is 0.98. In Figure 6b, the same plot is made for the descending branch of cycle 21 without time shift. Though the correlation coefficient is still high enough (0.79), the correlation is strongly nonlinear, and one can see strong deviations. Introducing a time shift does not improve the situation. Finally, Figure 7 shows the relation of the above-mentioned parameters without time shift for the period from 1979 to 1989: The black and the blue curves correspond to the ascending and the descending branches of cycle 22, respectively. One can clearly see a hysteresis-like structure. However, this result was obtained by comparing data from different spacecraft. Unfortunately, we could not study the behavior of CME parameters in the declining phase of cycle 22, because the data for the period of 1990 – 1996 are missing. In that period, active space missions with onboard coronagraphs were unavailable, and CME

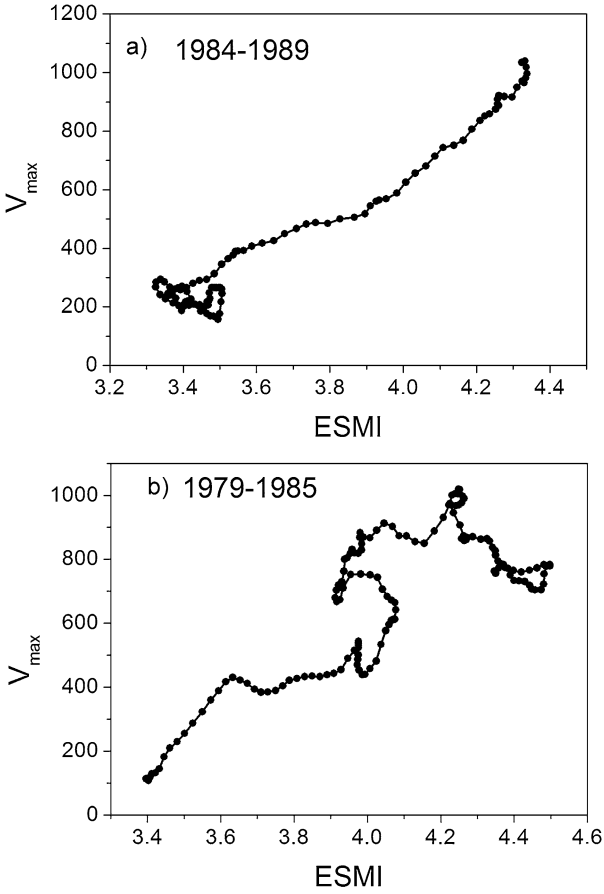

Figure 6 (a) V_{max} as a function of ESMI for the ascending branch of cycle 22 (the velocity data are shifted back in time by 14 half-rotations). (b) The same plot for the descending branch of cycle 21 without time shift.

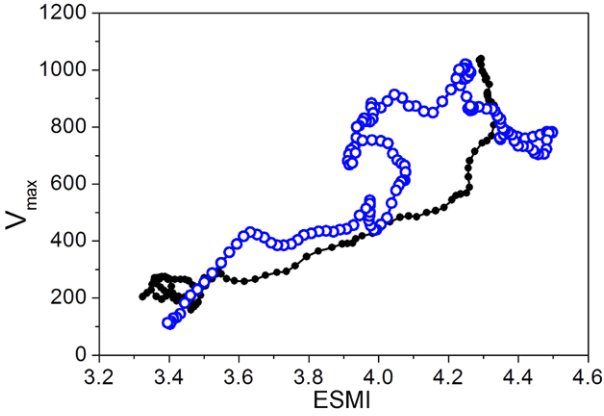

Figure 7 V_{max} as a function of ESMI without time shift for the period from 1979 to 1989. The black and the blue curves correspond to the ascending and the descending branches of cycle 22, respectively.

events were not recorded. The same effect, however, was revealed in cycle 23 when all observations were performed with one instrument.

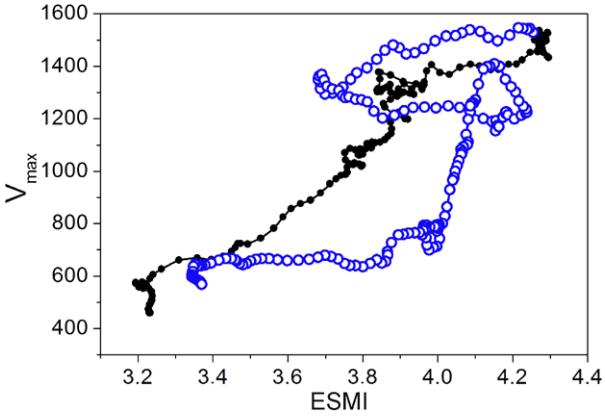

Figure 8 V_{max} as a function of ESMI for the period of 1996 – 2009. The black and the blue curves correspond to the ascending and the descending branches of cycle 23, respectively.

6. Evolution of LSMF Structure and CME Maximum Velocity in Different Phases of Cycle 23

Figure 8 shows the relationship between V_{max} and ESMI for the ascending (black) and descending (blue) branches of cycles 23, respectively. One can clearly see a hysteresis-type structure. Both the Maximum Coronal Mass Ejection Speed Index (MCMESI) and the geomagnetic activity reached their maximum values in the middle of 2002. The figure was plotted without a time shift of velocity relative to ESMI. The points follow at intervals equal to half a Carrington rotation (≈ 13.63 days). The ascending branch displays a pronounced linear relation with a high correlation coefficient (0.97). In this phase, all indices agree, as seen in Figure 3. On the descending branch, the linear relation is absent, though the formal correlation coefficient remains high (0.59). If we shifted the data for the descending branch (blue curve) by 67 half-rotations, the correlation coefficient would increase to 0.83 but the relation would remain intricate and involve a lot of deviations from linearity.

The comparison of variations in the CME maximum velocity (V_{max}) and ESMI over cycle 23 (Figure 3a) with similar variations of V_{max} as a function of ESMI (Figure 8) allows us to study in more detail the relationship between the behavior of the CME maximum velocity and the evolution of LSMF structure in different phases of an activity cycle. Comparing Figures 3a and 8, we can follow the evolution of the LSMF structure and CME maximum velocity over Cycle 23.

i) 1996.0 – 2001.4: The typical dimensions of the LSMF structure decreased noticeably, and the CME maximum velocity increased synchronously (almost linearly) up to ≈ 1500 km s^{-1}. A certain deviation in the cyclic curves was observed only in the period of 1999.8 – 2000.3, when the ESMI (multipole) index decreased (the typical dimensions of the LSMF structure increased), while the CME maximum velocity increased.

ii) 2001.4 – 2003.4: The typical dimensions of the LSMF structure increased noticeably, while the CME maximum velocity decreased but insignificantly (down to ≈ 1300 km s^{-1}).

2003.4 – 2004.5: The typical dimensions of the LSMF structure decreased noticeably, while the CME maximum velocity decreased but insignificantly (down to ≈ 1200 km s^{-1}).

iii) 2004.5 – 2005.0: A short period when both the typical dimensions of the LSMF structure and the CME maximum velocity increased. Note that in the same time interval,

both the large sunspot group numbers and geomagnetic indices (Ap and Dst) peaked correspondingly (see Figure 4 in Kilcik *et al.* (2011a)).

iv) 2005.0 – 2006.3: The typical dimensions of the LSMF structure increased slightly, and the maximum CME velocity decreased significantly (from ≈ 1400 down to 700 km s^{-1}).

v) 2006.3 – 2008.8: The typical dimensions of the LSMF structure increased significantly, while the decrease of the CME maximum velocity was relatively small (from ≈ 800 to 600 km s^{-1}). This trend was violated for a short time in the period of 2006.3 – 2006.8 when the CME maximum velocity increased slightly (from ≈ 700 to 800 km s^{-1}).

7. Conclusions

We have established for certain that CME parameters (velocity and occurrence rate) depend on cyclic variations of the LSMF structure, which determines the conditions for the formation of active complexes responsible for the occurrence of major CMEs. Therefore, the long-term CME forecast must take into account the indices that characterize the behavior of the large-scale solar magnetic field, in particular, the ESMI index considered above. The relationship between the occurrence of major, high-speed CMEs and the formation of active complexes does not rule out the possibility that weaker CMEs may be directly associated with certain local sources. This is evidenced, in particular, by the local maximum of low-speed CMEs at the end of cycle 23, when the conditions for the formation of active complexes became strongly unfavorable due to a noticeable increase in the LSMF size. As a result, the relative number of individual CME sources (not connected to activity complexes) seems to have increased in spite of the general decrease of activity. In each of the two main field systems (open and closed fields), the energy grows or decreases during the solar cycle. The distribution of energy between the systems also varies.

The figures presented above demonstrate clearly the similarity of cyclic variations of the occurrence rate and maximum velocity of CME and the ESMI (multipole) index. It is likely that the multipole index reflects the contribution from local and medium-scale fields. In the rising phase and maximum of the cycle, the local fields of active regions seem to make the greatest contribution. In the declining phase, the contribution from active regions decreases while that from intermediate fields remains relatively large. With the latter we associate the giant cells and coronal holes. This effect was particularly well-marked in cycle 23, when an extraordinarily large number of equatorial coronal holes and high-speed streams were observed in the declining phase (Tokumaru *et al.*, 2009). In the period from 2007 to 2009, the CME occurrence rate and intensity (velocity) are determined rather by individual active regions (sunspots) and eruptive filaments than by AR complexes as they did at the maximum and in the early rising phase. This, obviously, explains a relative growth of the CME occurrence rate in that period and their low speed, which did not usually exceed 700 km s^{-1}.

As follows from the description above, noticeable variations in the CME maximum velocity occurred in the rising phase (from 1996.0 to 2001.4) and in the second half of the declining phase of cycle 23 (from 2005.0 to 2008.8). In the period of 2001.4 – 2005.0, the CME maximum velocity remained high enough ($\approx 1400 - 1500$ km s^{-1}), probably, because that was the period when complexes of activity connected by coronal arch systems and responsible for the generation of major geoeffective CMEs were most frequently recorded.

The hysteresis described by Özgüç, Kilcik, and Rozelot (2012) is due to the fact that the fields of different scales make different contributions to the general magnetic flux in different phases of the cycle. In the rising phase, the curves of the multipole index and SSN are similar. In the declining phase, the multipole index decreases much more slowly

than SSN, which results in a hysteresis. Note that the delay of the multipole index in the declining phase increased gradually in the recent cycles. In cycle 21, it was ≈ 1 year; in cycle 22, it increased to 1.5 years; and in cycle 23, it was 3 – 4 years.

Cycle 23 was abnormal in many respects (Obridko and Shelting, 2009), including the behavior of the multipole index. In 2003, it dropped rapidly, and one might expect that, in analogy with the previous cycles, it would continue decreasing down to the minimum values. However, this was not the case. In 2004, the index increased significantly and almost reached the values typical of the cycle maximum, undoubtedly, because of an essential increase of the medium-scale fields. This determined a large hysteresis in cycle 23.

It is interesting to note that the beginning of cycle 24 was characterized by a fast increase in the multipole index – much faster than the increase in SSN. This was, obviously, due to a large number of equatorial coronal holes, unusual in this phase. It is not clear so far how this may tell on the amplitude of cycle 24. If the decreasing tendency in the maximum ESMI value (and the corresponding increase in the characteristic dimensions of the elements of the large-scale solar magnetic field at the maximum) continues in cycle 24, we expect that the relative number of major, high-speed CMEs and, thus, their damaging effect on the technological systems on the Earth will decrease at the maximum of cycle 24 (2012 – 2013).

Acknowledgements This work was conducted under the sponsorship of the Russian Foundation for Basic Research (grant N 11-02-00259).

References

Burkepile, J.T., St. Cyr, O.C.: 1993, *A Revised and Expanded Catalogue of Mass Ejections Observed by the Solar Maximum Mission Coronograph*, High Altitude Observatory, NCAR, Boulder.
Bumba, V.: 1976, In: Bumba, V., Kleczek, J. (eds.) *Basic Mechanisms of Solar Activity, IAU Symp.* **71**, 47.
Bumba, V.: 1986, *Bull. Astron. Inst. Czechoslov.* **37**, 281.
Bumba, V., Gesztelyi, L.: 1988, *Bull. Astron. Inst. Czechoslov.* **39**, 86.
Bumba, V., Obridko, V.N.: 1969, *Solar Phys.* **6**, 104.
Chertok, I.M., Belov, A.V., Grechnev, V.V.: 2011, *Bull. Russ. Acad. Sci., Phys.* **75**, 796.
Chertok, I.M., Grechnev, V.V.: 2005, *Solar Phys.* **229**, 95.
Hoeksema, J.T., Scherrer, P.H.: 1986, *Solar Magnetic Field-1976 through 1985, Report UAG-94*, World Data Center A for Solar-Terrestrial Physics, Boulder, CO.
Danilchev, B.V., Morozova, L.P., Obridko, V.N.: 1986, *Soln. Dannye* **4**, 69.
Donnelly, R.: 1992, In: Donnelly, R.F. (ed.) *Proc. Workshop on the Solar Electromagnetic Radiation Study for Solar Cycle 22*, NOAA, Boulder, 275.
Grechnev, V.V., Chertok, I.M., Slemzin, V.A., Kuzin, S.V., Ignat'ev, A.P., Pertsov, A.A., Zhitnik, I.A., Delaboudinière, J.-P., Auchère, F.: 2005, *J. Geophys. Res.* **110**, A09S07.
Howard, R.A., Sheeley, N.R. Jr., Koomen, M.J., Michels, D.J.: 1991, *Preliminary CME List, Washington.* http://lasco-www.nrl.navy.mil/solwind_transient.list.
Ivanov, E.V.: 1986, *Soln. Dannye* **7**, 61.
Ivanov, E.A.: 1994, In: Baker, D.N., Papitashvili, V.O., Teague, M.J. (eds.) *Solar Terrestrial Energy Program. The Initial Results from STEP Facilities and Theory Campaigns*, *COSPAR Colloq. Ser.* **5**, Pergamon, New York, 133.
Ivanov, E.V.: 1995, *Bull. Russ. Acad. Sci., Phys.* **59**, 1133.
Ivanov, E.V., Obridko, V.N., Shelting, B.D.: 1997, *Astron. Rep.* **41**, 236, translated from *Astron. Zh.* **74**, 273.
Ivanov, E.V., Obridko, V.N., Shelting, B.D.: 1998, In: Feng, X.S., Wei, F.S., Dryer, M. (eds.) *Advances in Solar Connection with Interplanetary Phenomena, Proc. Third SOLTIP Symp.*, International Academic Publishers, Beijing, 365.
Ivanov, E.V., Obridko, V.N., Nepomnyashchaya, E.V., Kutilina, N.V.: 1999, *Solar Phys.* **184**, 369.
Ivanov, E.V.: 2007, *Adv. Space Res.* **40**, 959.
Kilcik, A., Yurchyshyn, V.B., Abramenko, V., Goode, P.R., Gopalswamy, N., Özgüç, A., Rozelot, J.P.: 2011a, *Astrophys. J.* **727**, 44.
Kilcik, A., Yurchyshyn, V.B., Abramenko, V., Goode, P.R., Ozgüç, A., Rozelot, J.P., Cao, W.: 2011b, *Astrophys. J.* **731**, 30.

Kuklin, G.V.: 1971, In: Howard, R. (ed.) *Solar Magnetic Fields*. *IAU Symp.* **43**, 737.
Kuklin, G.V., Obridko, V.N.: 1989, In: *Solar-Terrestrial Energy Program: Major Scientific Problems*, University of Illinois, Urbana, 7.
Makarov, V.I., Sivaraman, K.R.: 1989a, *Solar Phys.* **119**, 35.
Makarov, V.I., Sivaraman, K.R.: 1989b, *Solar Phys.* **123**, 367.
Obridko, V.N.: 1984, *Soln. Dannye* **11**, 54.
Obridko, V.N., Ermakov, F.A.: 1989, *Astron. Tsirk* **1539**, 24.
Obridko, V.N., Kuikin, G.V.: 1993, In: Hruska, J., Shea, M.A., Smart, D.F., Heckman, G. (eds.) *Solar-Terrestrial Predictions Workshop IV* **2**, 273.
Obridko, V.N., Shelting, B.D.: 1987, *Geomagn. Aeron.* **27**, 660.
Obridko, V.N., Shelting, B.D.: 1992, *Solar Phys.* **137**, 167.
Obridko, V.N., Shelting, B.D.: 2009, *Astron. Lett.* **35**, 247.
Obridko, V.N., Shelting, B.D.: 2011, *Solar Phys.* **270**, 297.
Obridko, V.N., Shelting, B.D., Livshits, I.M., Asgarov, A.B.: 2009, *Solar Phys.* **260**, 191.
Özgüç, A., Ataç, T.: 2002, In: Wang, H.N., Xu, R.I. (eds.) *Solar-Terrestrial Magnetic Activity and Space Environment*, *COSPAR Colloq. Ser.* **14**, Pergamon, Boston, 447.
Özgüç, A., Kilcik, A., Rozelot, J.P.: 2012, *Solar Phys*. doi:10.1007/s11207-012-0087-5.
Reinard, A.A., Biesecker, D.A.: 2009, *Astrophys. J.* **705**, 914.
Shelting, B.D., Obridko, V.N.: 1988, *Kinemat. Fiz. Nebesnyh Tel* **4**, 29.
Tokumaru, M., Kojima, M., Fujiki, K., Hayashi, K.: 2009, *Geophys. Res. Lett.* **36**, L09101.
Vitinsky, Yu.I., Kuklin, G.V., Obridko, V.N.: 1986, *Soln. Dannye* **3**, 53.
Zhang, Y., Wang, J., Attrill, G.D.R., Harra, L.K., Yang, Z., He, X.: 2007, *Solar Phys.* **241**, 329.